This article has been accepted for publication in a future issue of this journal, but has not been fully edited. Content may change prior to final publication. Citation information: DOI 10.1109/ACCESS.2017.2703876, IEEE Access

Directive Beam of the Monopole Antenna Using Broadband Gradient Refractive Index Metamaterial for Ultra-Wideband Application

Rahul Singha, *Student member, IEEE*, D. Vakula

***Abstract*—These This paper introduces a novel techniques to enhance the gain of the basic monopole antenna by using broadband gradient refractive index (GRIN) metamaterial. The proposed GRIN is designed by using parallel-line unit cell metamaterial with different refractive index. A seven GRIN lens is placed on the omnidirectional printed basic monopole antenna, perpendicularly. Due to the non-resonant and subwavelength properties of the parallel-line elements, the proposed GRIN metamaterial lens has a broad bandwidth property with low loss. The simulation and measurement results confirmed that the beam is more directive with narrow beam width. The measured reflection coefficient of the GRIN antenna is below –10 dB over the frequency bandwidth of 3.4 to 11 GHz. Due to GRIN lens, the peak gain of the basic monopole antenna is increased by 5.3 dB at 8.8 GHz.**

***Index Terms*—Monopole Antenna, subwavelength, metamaterial, gradient refractive index, lens.**

I. Introduction

The necessity of the ultra-wideband (UWB) antenna is significantly increased in the field of defense and commercial applications. Compared to other UWB antennas, the printed monopole antenna has several advantages such as planar structure, light weight, compact size, low cost, ease of fabrication and capable of integration with electronics system. At the same time, the antenna is suffering from low gain characteristics, and it depends on the size of the antenna. A common solution is the antenna array technique to enhance the gain which usually results in coupling between antennas, high cost or much trouble for designers.

In past decades, many engineers and scientists have widely used metamaterial based circuits in the superstrate [2], [3], artificial magnetic conductor (AMC) [3], [4] etc. to enhance the gain of the antennas, which have limited bandwidth with large losses for electric or magnetic resonant metamaterials. Moreover, circuit complexity makes fabrication very complicated and costly. To overcome this problem, the gradient-index (GRIN) metamaterials is very useful with low loss and broad bandwidth, whose refractive index changes gradually according to the geometry of devices.

The first GRIN metamaterial was implemented by D. R. Smith in 2005, based on conducting split-ring resonators (SRRs) to confirm the gradient by measuring the deflection of a microwave beam [5]. Later, it is used in waveguide [6], microwave (horn) antenna [7], planar antenna [8]. Due to the beam focusing property, the zero index metamaterial and gradient index designs are used in antenna to create a unidirectional beam [17]-[19]. However, most of the existing GRIN works do not cover UWB frequency range.

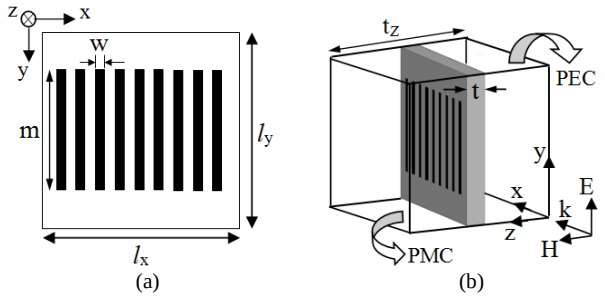

Fig. 1 The geometry of the artificial material (a) unit cell, (b) Simulation model. The dimensions of unit cell are $l_x = l_y = 6$ mm, $w = 0.2$ mm, $t = 0.8$ mm and $t_z = 6$ mm.

In this work, a gradient refractive index (GRIN) metamaterial lens is designed and integrated with monopole antenna. The lens is designed by using non-resonant parallel-line metamaterial. This non-resonant structure is covered UWB frequency range, which has the capability to enhance the gain of the proposed antenna. The peak gain of the basic monopole is increased approximately by five times for GRIN lens.

II. Design and Characteristics of GRIN Parallel-line Metamaterial

The unit cell metamaterial is designed by using non-resonant parallel metallic lines on the substrate as shown in Fig. 1(a). Because, the resonant metamaterial structures are lead to highly dispersive with considerable loss near the resonant frequency, which is not suitable for applications where broad bandwidth and low loss are required. So, the non-resonant metamaterial elements provides almost non-dispersive effective constitutive parameters with negligible

Rahul Singha is with the Department of Electronics and Communication Engineering, National Institute of Technology Warangal 506004, India (e-mail: ieee.rahul5488@gmail.com).

D. Vakula is with the Department of Electronics and Communication Engineering, National Institute of Technology Warangal 506004, India (e-mail: vakula@nitw.ac.in).

This article has been accepted for publication in a future issue of this journal, but has not been fully edited. Content may change prior to final publication. Citation information: DOI 10.1109/ACCESS.2017.2703876, IEEE Access

loss. The proposed material is fabricated on the single side of the dielectric material Roger RO4003 with dielectric constant 3.55, the thickness of 0.8 mm and loss tangent 0.0027. The dimensions of the unit cell has been taken as

$$l_x = l_y = \lambda_0 / 8.3$$

where $\lambda_0 = c/f * \sqrt{\varepsilon_r}$ at f=6 GHz. The dimension is chosen in terms of free space wavelength (λ_0) indicating that the EM wave will enter in metamaterial through the air.

To extract the values of effective parameter, the scattering object is replaced by a homogeneous medium i.e. the wavelength within the medium becomes large in terms of the unit cell size [10], [11]. To evaluate the scattering performance, the simulation model of the single unit cell is shown in Fig. 1(b). The perfect electric conductor (PEC) and perfect magnetic conductor (PMC) boundary conditions are also defined. The electric and magnetic polarizations are along the y and z-axes, respectively. The EM wave will propagate along the x-axis.

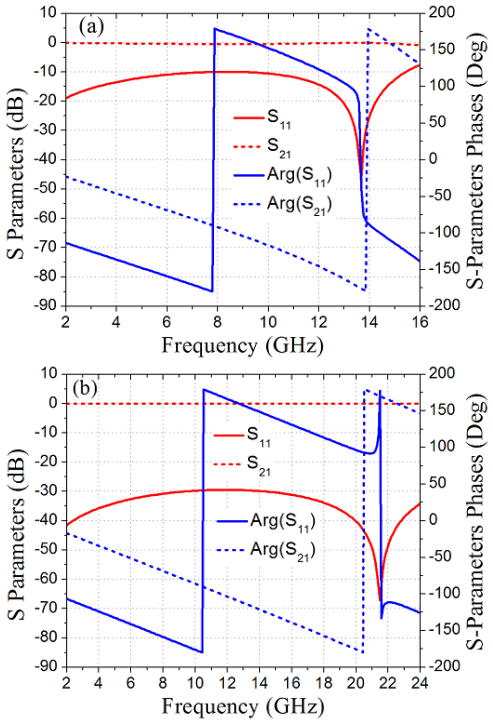

Fig. 2. Magnitude (red color) and phase response (blue color) of the scattering parameters for (a) m=4 mm, and (b) m=1.1 mm.

The effective parameters are a refractive index (n), permittivity (ε_y) and permeability (μ_z) extracted from the magnitude and phase of the scattering parameters using standard retrieval procedure described [13], [14]. From the Fig. 1(a), it can be seen that the length of the parallel metallic line is m. Fig. 2 illustrates the lowest and highest resonant frequencies are 14 GHz and 22 GHz obtained by choosing m=4 mm and m=1.1 mm, respectively. The corresponding effective permittivity and permeability data's are plotted as shown in Fig. 3(a) and (b), respectively. The effective refractive index values are also plotted, depicted in Fig. 3(c). Since, the current path of the parallel-line metamaterial is different for various values of m. So, the resonant frequency of the proposed material is changing with the length of m. At the same time, it can be also observed that effective permittivity values are also changing for the value of m. But the effective permeability values are not varying significantly. Obviously, the refractive index values are also changing simultaneously.

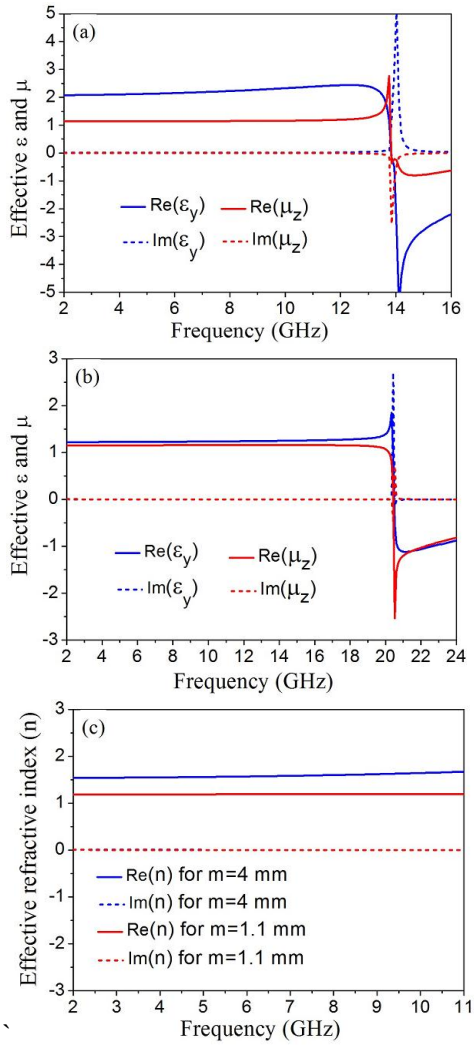

Fig. 3. Effective permittivity (ε_y) and permeability (μ_z) of the metamaterial unit cell for (a) m=4 mm, and (b) m=1.1 mm, and (c) Effective refractive index for m=4 mm, m=1.1 mm.

From the Fig. 3(c), it can be noticed that the refractive index is not constant over the frequency band from 2–11 GHz. The variation of the effective refractive index over the frequency band from 2–11 GHz is shown in Table I which indicates that the refractive index values are also changing with different values of m. So, the effective refractive index is calculated by taking the average of the refractive index for a given frequency band at different values of m and these average refractive index data's are plotted as shown in Fig. 4.

This article has been accepted for publication in a future issue of this journal, but has not been fully edited. Content may change prior to final publication. Citation information: DOI 10.1109/ACCESS.2017.2703876, IEEE Access

TABLE I
VARIATION OF EFFECTIVE REFRACTIVE INDEX

Frequency range	Parallel-line unit cell length, *m*	Variation of Effective Refractive Index, *n*
2–11 GHz	4 mm	1.53–1.67
	3.7 mm	1.47–1.58
	3.4 mm	1.42–1.5
	3.1 mm	1.37–1.42
	2.9 mm	1.34–1.38
	2.7 mm	1.31–1.35
	2.4 mm	1.29–1.32
	2.1 mm	1.25–1.27
	1.8 mm	1.23–1.24
	1.5 mm	1.2–1.22
	1.1 mm	1.18–1.19
	0.5 mm	1.1–1.15

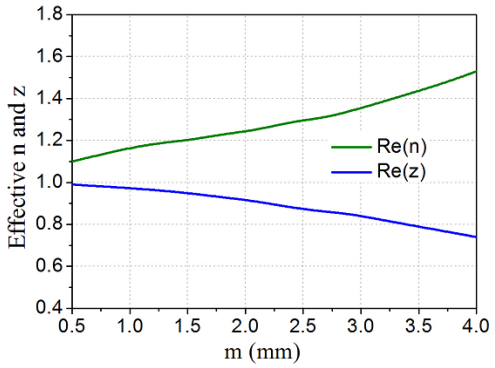

(a)

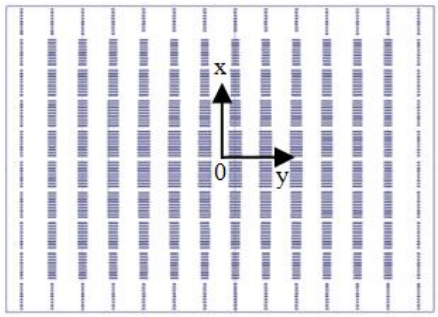

(b)

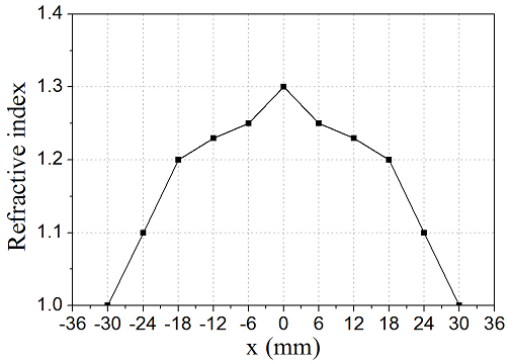

(c)

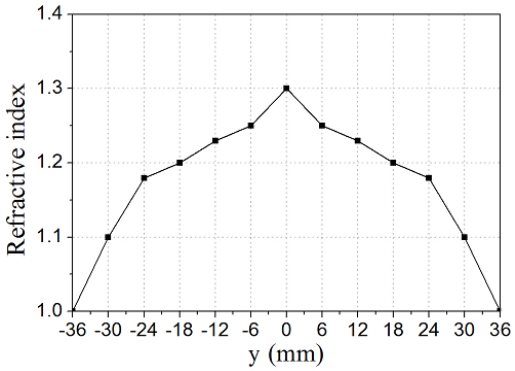

(d)

Fig. 4 Retrieval results for the parallel line medium, (a) The relationship between the extracted refractive index (*n*) and wave impedance (*z*) on length *m*, (b) The schematic graph of the metallic parallel-lines, (c) The refractive-index distribution along x-direction, and (d) The refractive-index distribution along y-direction.

To understand the effect of m, the simulations of the unit cell is analyzed with different lengths of *m*. Fig. 4(a) shows the variation of effective refractive index and impedance of the unit cell parallel-line metamaterial for the various values of *m*. From the figure, it is observed that the effective refractive index value becomes low by decreasing the length of the parallel metallic line, *m*. The effective impedance values are near to the unity when the values of m are becoming low. The schematic design of the GRIN lens by using parallel-line metamaterial is shown in Fig. 4(b). The refractive index distribution in GRIN lens is very important to create a minimum reflection. The dimension of the GRIN lens is 84×60 mm^2. According to the refractive index values, the arrangement of the metamaterial unit cell in the GRIN lens along the x and y-directions is shown in Fig. 4(c) and (d), respectively. The GRIN metamaterial lens is placed above the basic monopole to amplify the EM wave in the direction of the x-axis.

III. DESIGN OF GRIN INTEGRATED BASIC MONOPOLE ANTENNA

The geometry of the proposed basic monopole antenna is shown in Fig. 5(a). The top and bottom conductor is denoted by dark and light grey color. The antenna is designed and etched on the roger RT/duroid 5880 substrate with dielectric constant 2.2 and thickness, *h*=0.787 mm. The excitation of the antenna is given by using 50 Ω microstrip line feed with line width 2 mm and bottom layer consists of the partial ground. The size of the basic monopole is 25×28 mm^2.

In the proposed design, the bottom part of the radiating patch is responsible for the variation of the antennas lowest frequency (f_L). In that place, the polygon structure is designed with an angle (θ) on the radiating patch. The angle θ must vary to fix f_L of the UWB frequency range. The current distribution on the partial ground layer is also responsible for impedance matching of the antenna. Here, the current path of the ground part can be controlled by varying the parameter *d*.

This article has been accepted for publication in a future issue of this journal, but has not been fully edited. Content may change prior to final publication. Citation information: DOI 10.1109/ACCESS.2017.2703876, IEEE Access

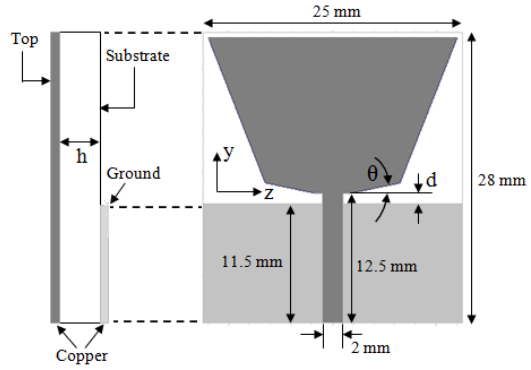

(a)

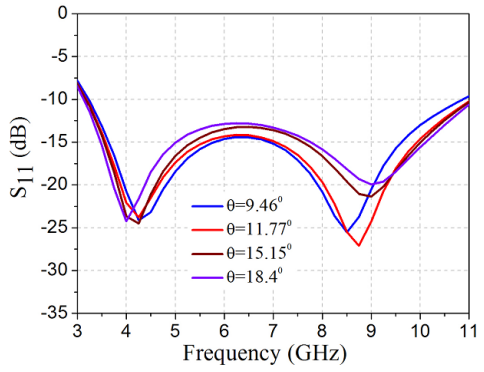

(b)

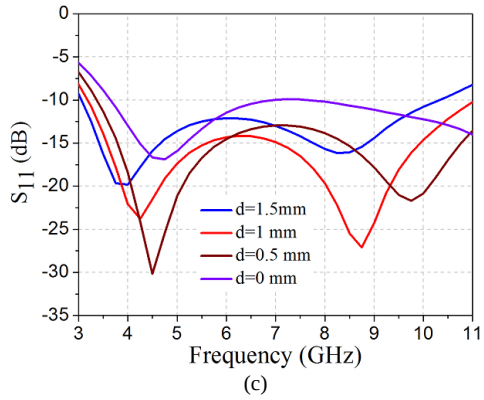

(c)

Fig. 5 Geometry of the basic monopole antenna and its analysis, (a) Top and side view of the basic monopole, (b) Reflection coefficient (S_{11}) for different value of θ, (c) Reflection coefficient (S_{11}) for different value of d.

Fig. 5(b) illustrates the effect of f_L by changing the angle θ. The f_L is shifted slightly left side for the increment of θ. The Fig. 5(b) is also indicating that the reflection coefficient is gradually increasing in the middle of the operating frequency band. At θ=11.77^0, the f_L and other frequencies are well maintained over UWB frequency range. The fluctuation of S_{11} for another parameter d at θ=11.77^0 is shown in Fig. 5(c). It is clear that the lowest frequency f_L is decreasing with increasing the values of d. At the same time, the S_{11} is also increasing at high frequencies. The f_L=3.1 GHz after optimizing the values of θ and d are 11.77^0 and 1 mm, respectively.

To design GRIN antenna, the seven GRIN lenses are placed on the basic monopole antenna as shown in Fig. 6(a). The antenna and GRIN lens are separated by rohacel foams. The distance from the radiation source to the bottom of the GRIN lens is 23 mm. The near-field coupling between the GRIN and the basic monopole is not affected significantly. At the same time, the distance between the corresponding GRIN lens is kept 4 mm (>l_x/2) to avoid the destruction of metamaterial properties. Fig. 6(b) illustrates the simulated reflection coefficient (S_{11}) of the optimized basic monopole and the GRIN monopole antenna. It can be seen that the f_L is slightly shifted towards the right side.

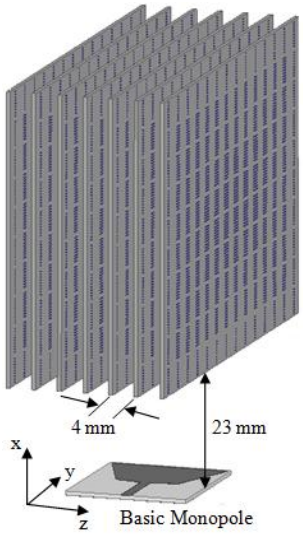

(a)

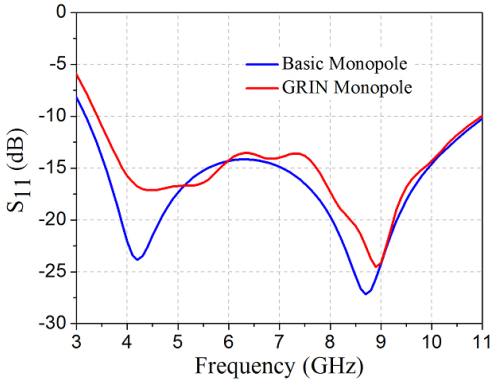

(b)

Fig. 6 The arrangement of the GRIN with basic monopole, (a) View of GRIN monopole, (b) Simulation result of the reflection coefficient (S_{11}) optimized basic and GRIN monopole.

TABLE II
COMPARISON OF THE PERFORMANCE OF THE PROPOSED GRIN MONOPOLE WITH SIMILAR PUBLISHED WORKS

Ref.	-10dB impedance bandwidth	Peak gain increment	Overall dimension
[8]	3-8 GHz	11 dB	n/a
[9]	6.7-12 GHz	9.5 dB	n/a
[15]	10.5-12.5 GHz	n/a	n/a
[16]	8.9-10.8 GHz	4 dB	215×139×85.8 mm^3
Proposed structure	3.4-10.6 GHz	5.3 dB	170×125×100 mm^3

This article has been accepted for publication in a future issue of this journal, but has not been fully edited. Content may change prior to final publication. Citation information: DOI 10.1109/ACCESS.2017.2703876, IEEE Access

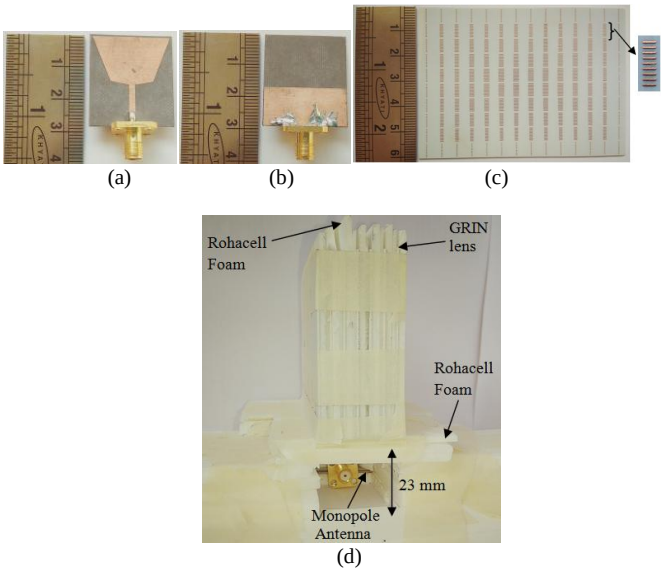

Fig. 7 Photograph of the fabricated antennas (a) Top view, (b) Bottom view, (c) GRIN lens, (d) Seven GRIN lens on the antenna.

IV. Results and Discussions

The proposed antennas are optimized by simulating a three-dimensional electromagnetic (EM) simulator CST microwave studio 2015. The fabricated prototype of the basic and GRIN monopole antennas are shown in Fig. 7. The comparison of the proposed GRIN antenna with some existing works in terms of size, operating frequency band, the peak gain increment is shown in Table II. The proposed GRIN antenna has a more compact size compared to the other published works and also working on UWB characteristics.

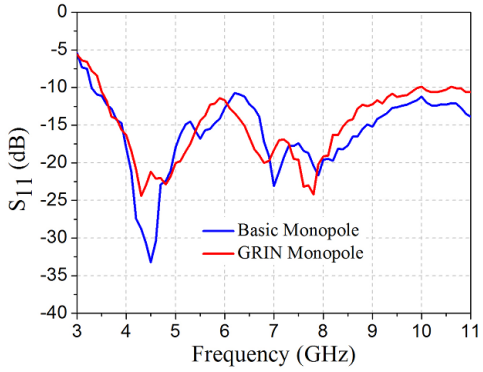

Fig. 8 Measured reflection coefficient (S_{11}) of the antennas.

Fig. 8 shows the measured reflection coefficient (S_{11}) of the basic and GRIN monopole antennas. It is clearly evident that the S_{11} of the basic and GRIN monopole are less than -10 dB covering a bandwidth of 3.1–11 GHz and 3.4-11 GHz, respectively. In the case of GRIN antenna, the f_L is 3.4 GHz, and the S_{11} is fluctuating near -10 dB over bandwidth 10-11 GHz. Here, the measurement result of f_L is giving different value, because the 3D EM software has been taken as an ideal structure filled by air between the objects. But the photograph of GRIN antenna is supported and fixed by using rohacel foams and paper tape. Therefore, the measured data is slightly different from the simulation result.

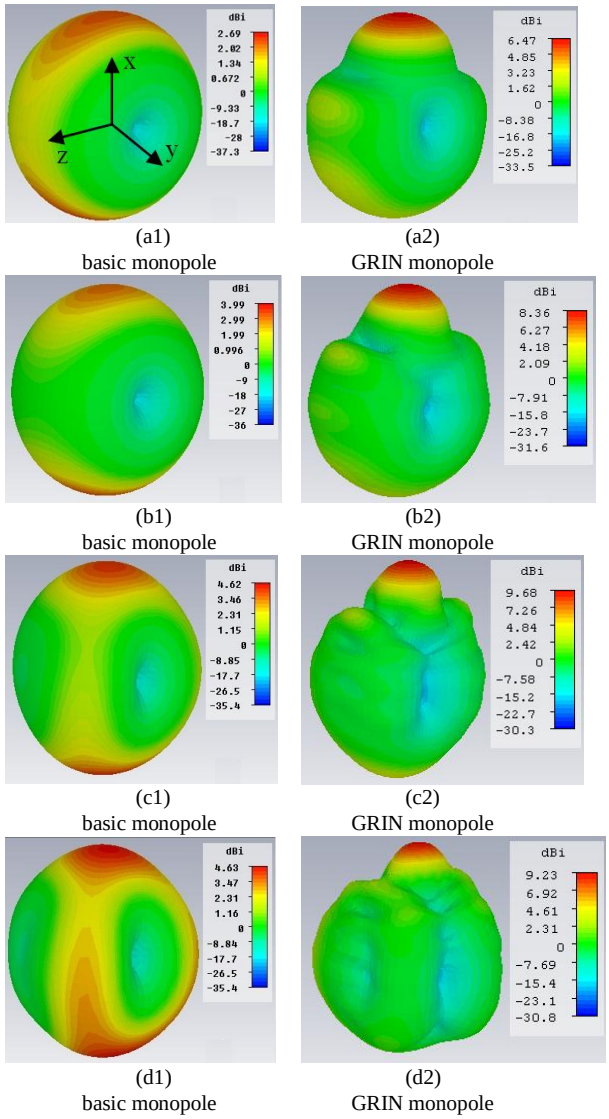

Fig. 9 Simulated 3D far-field radiation patterns. For basic monopole at (a1) 4.5 GHz, (b1) 6.2 GHz, (c1) 8 GHz, (d1) 10 GHz and GRIN monopole at (a2) 4.5 GHz, (b2) 6.2 GHz, (c2) 8 GHz, (d2) 10 GHz.

Fig. 9 illustrates the simulated 3D far-field radiation patterns of the monopole without and with GRIN lenses. From the figure, it can be seen that a single beam directive 3D radiation pattern is maximum in the direction of x-axis at 4.5 GHz, 6.2 GHz, 8 GHz and 10 GHz. The omnidirectional patterns of the basic monopole in xz-plane (H-plane) are transformed to single narrow beam patterns with directive emission.

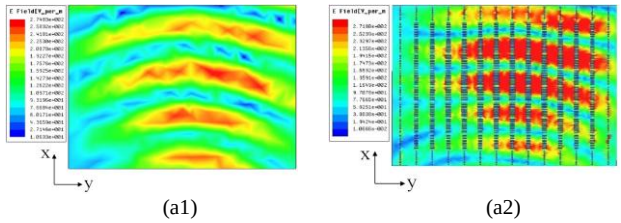

This article has been accepted for publication in a future issue of this journal, but has not been fully edited. Content may change prior to final publication. Citation information: DOI 10.1109/ACCESS.2017.2703876, IEEE Access

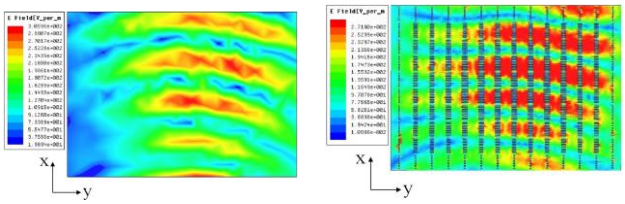

(b1) (b2)

Fig. 10 Simulated electric-field distributions in free space with and without unit cell metamaterial structure in GRIN lens. Without unit cell structure in GRIN lens at (a1) 9 GHz, (b1) 10 GHz, and with unit cell structure in GRIN lens at (a2) 9 GHz, (b2) 10 GHz.

In order to understand the effect of GRIN, the GRIN monopole is simulated in the 3D EM software HFSS 15. Fig. 10 shows the free-space electric-field distributions with and without unit cell metamaterial structure in GRIN lens. So, it can be observed that the quasi-spherical waves are almost converted into the plane waves in the direction of the x-axis at 9 and 10 GHz by comparing the wavefronts outgoing through with and without unit cell structures in the GRIN lens. Since the GRIN elements operate far from their resonant frequencies, the loss induced by the sample is low. Therefore, the color maps of the outgoing waves are showing almost identical intensity for with and without parallel-line metamaterial.

The measured H–plane (xz plane) patterns of the antennas are compared at 4.5 GHz, 6.2 GHz, 8 GHz and 10 GHz as shown in Fig. 11. The measurement result is indicating that the radiation patterns are improved by using GRIN lens in basic monopole antenna and more directive. Fig. 11(e) shows the measured peak gain of the basic monopole and GRIN monopole antennas in the beam direction of the x-axis. So, it is clear that the peak gain of the basic monopole has been increased by 5.3 dB at 8.8 GHz (approximately) due to the effect of GRIN lens and the gain of GRIN antenna is varying from 4.5-9.8 dB over the frequency band of 3−10 GHz.

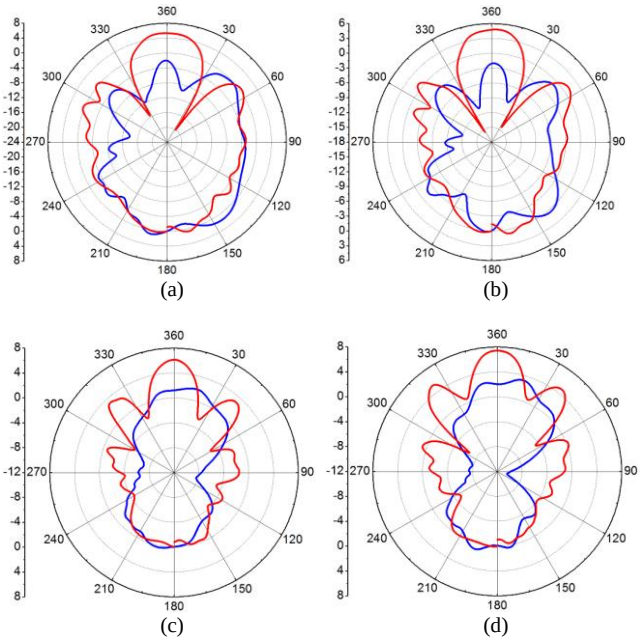

(a) (b) (c) (d)

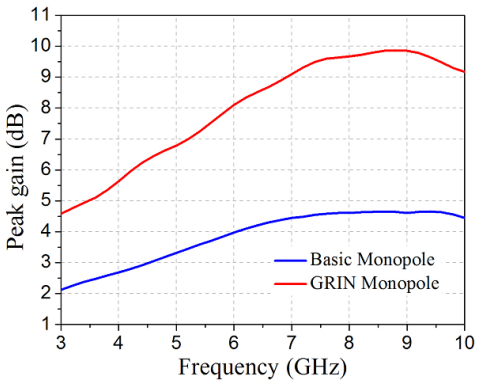

(e)

Fig. 11 Measured H-plane radiation patterns at (a) 4.5 GHz, (b) 6.2 GHz, (c) 8 GHz, (d) 10 GHz and (e) Measured gain variation of the basic monopole and GRIN monopole antenna. The blue and red solid line denotes a basic monopole and GRIN monopole, respectively.

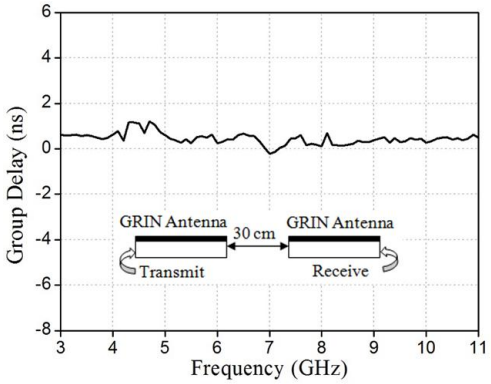

Fig. 12 Group delay performance of the GRIN monopole antenna

For UWB antenna, the frequency dependent parameters are not sufficient. Therefore, the time domain characteristic of the fabricated GRIN monopole is tested. So, two GRIN antennas are arranged side by side with a distance 30 cm and connected to the ports of the vector network analyzer (VNA). Fig. 12 shows the antenna is giving almost stable group delay performance with a fluctuation approximately ±1.2 ns in the desired band, indicating that a transmitted signal will not be seriously distorted by the proposed antenna.

V. Conclusion

In this paper, a directive beam of the basic monopole antenna is augmented with a broadband GRIN parallel-line metamaterial. The proposed GRIN based monopole has a compact size. The measured results of the fabricated antenna are showing that the gain of the basic monopole is increased by 5.3 dB at 8.8 GHz. The operating frequency band of the antenna is not significantly affected by using GRIN. Hence, the proposed antenna is a good candidate for ultra-wideband communication systems.

References

[1] Federal Communications Commission: First Report and Order on Ultra-Wideband Technology, FCC 02 –48, Washington, DC, 2002.

[2] F. H. Wee, F. Malek, A. U. Al-Amani, and F. Ghani, "Effect of two different superstrate layers ON Bismuth Titanate (BiT) array antennas," *Sci. Rep*., vol. 4, p. 3709, Jan. 2014.
[3] Arand, B.A., Bazrkar, A., "Gain Enhancement of a Tetra-band Square-Loop Patch Antenna Using an AMC–PEC Substrate and a Superstrate," *Wireless Pers. Commun*., vol. 84, no. 1, pp. 87-97, 2015.
[4] P. Prakash, M. P. Abegaonkar, A. Basu, and S. K. Kou, "Gain enhancement of a CPW-fed monopole antenna using polarization-insensitive AMC structure," *IEEE Antennas Wirel. Propag. Lett*., vol. 12, pp. 1315–1318, 2013.
[5] D. R. Smith, J. J. Mock, A. F. Starr, and D. Schurig, "Gradient index metamaterials," *Phys. Rev. E*, vol. 71, pp. 036609-1–036609-6, 2005.
[6] Fu, Y., Xu, Y. & Chen, H., "Applications of gradient index metamaterials in waveguides," *Sci. Rep*., vol. 5, p. 18223, 2015.
[7] C. Xi, H. F. Ma, Y. Z. Xia, and W. J. Jiang, "Three-dimensional broadband and high-directivity lens antenna made of metamaterials," *J. Appl. Phys*., vol. 110, pp. 044904–044904-8, Aug. 2011.
[8] H.-X. Xu, G.-M. Wang, Z. Tao, and T.-J. Cui, "High-directivity emissions with flexible beam numbers and beam directions using gradientrefractive-index fractal metamaterial," *Sci. Rep*., vol. 4, p. 5744, 2014.
[9] E. Erfani, M. Niroo-Jazi, and S. Tatu, "A high-gain broadband gradient refractive index metasurface lens antenna," *IEEE Trans. Antennas Propag*., vol. 64, no. 5, pp. 1968–1973, May 2016.
[10] R. Liu, T. J. Cui, D. Huang, B. Zhao, and D. R. Smith, "Description and explanation of electromagnetic behaviors in artificial metamaterials based on effective medium theory," *Phys. Rev. E*, vol. 76, p. 026606, Aug. 2007.
[11] L. Chen, Z. Lei, R. Yang, J. Fan, X. Shi, "A broadband artificial material for gain enhancement of antipodal tapered slot antenna," *IEEE Trans. Antennas Propag*., vol. 63, no. 1, pp. 395–1746, 2015.
[12] Qi, M. Q., Tang, W. X., Ma, H. F., Pan, B. C., Tao, Z., Sun, Y. Z., Cui, T. J., "Suppressing side-lobe radiations of horn antenna by loading metamaterial lens," *Sci. Rep*., vol. 5, pp. 1–6, 2014.
[13] D. R. Smith, D. C. Vier, T. Koschny, and C. M. Soukoulis, "Electromagnetic parameter retrieval from inhomogeneous metamaterials," *Phys. Rev. E*, vol. 71, no. 3, p. 036617, 2005.
[14] D. Li, Z. Szabó, X. Qing, E.-P. Li, and Z. Chen, "A high gain antenna with an optimized metamaterial inspired superstrate," *IEEE Trans. Antennas Propag.*, vol. 60, no. 12, pp. 6018–6023, Dec. 2012.
[15] Molina, H.B. and Hesselbarth, J., "Microwave dielectric stepped-index flat lens antenna," *Int. J. Microw. Wireless Technol*., pp. 1-7, 2016.
[16] F. Y. Meng, Y. L. Lv, K. Zhang, Q. Wu, and L. W. Li, "A detached zero index metamaterial lens for antenna gain enhancement," *Prog. Electromagn. Res*., vol. 132, pp. 463–478, 2012.
[17] H. X. Xu, G. M. Wang, Z. Tao, and T. Cai, "An octave-bandwidth half Maxwell fish-eye lens antenna using three-dimensional gradient-index fractal metamaterials," *IEEE Trans. Antennas. Propag*., vol. 62, no. 9, pp. 4823–4828, Sep. 2014.
[18] H.-X. Xu et al., "Miniaturization of 3-D anistropic zero-refractive-index metamaterials with application to directive emissions," *IEEE Trans. Antennas. Propag.*, vol. 62, no. 6, pp. 3141–3149, Jun. 2014.
[19] H.-X. Xu et al., "Multifunctional microstrip array combining a linear polarizer and focusing metasurface," *IEEE Trans. Antennas Propag*., vol. 64, no. 8, pp. 3676–3682, Aug. 2016.

Rahul Singha received his B.E. in Electrical and Electronics Engineering and M.Tech. in Microelectronics & VLSI design from National Institute of Technology (NIT) Agartala in the year 2010 and 2013, respectively. He is currently a Ph.D. student at the Dept. of Electronics and Communication Engineering, National Institute of Technology, Warangal. His research interests include Metamaterial, UWB antenna design, Microstrip filter.

Damera Vakula received her Bachelor's degree in Electronics and Communication Engineering from Nagarjuna University, AP, India and Master's degree .Tech. from Birla Institute of Technology, Mesra, India, with Microwave specialization in the year 1992 and 1994, respectively. She obtained Ph.D. on Fault diagnostics of Antenna Arrays from National Institute of Technology, Warangal, in the year 2010. She is working as assistant professor National Institute of Technology, Warangal, India since 2006. She has published 31 papers in international Conferences and Journals. Her areas of interests include Phase array antennas, Ultra wideband antennas, multiband antennas, fault diagnostics, and Neural network.